On the Formation Features and Some Material Properties of the Coating Formed by Laser Cladding of a NiCrBSi Self-fluxing Alloy

Oleg Devojno, Eugene Feldshtein, Marharyta Kardapolava and Nikolaj Lutsko

Abstract In the present paper, the influence of laser cladding conditions on the powder flow conditions as well as the microstructure, phases, and microhardness of a Ni-based self-fluxing alloy coating is studied. The formation regularities of a coating microstructure with different cladding conditions as well as patterns of element distribution over the coating depth and in the transient zone are defined. The microhardness distribution patterns by depth and length of a coating for various laser cladding conditions have been studied. It was found that the laser beam speed, track pitch, and the distance from the nozzle to the coated surface influence the changes of the coating microstructure and microhardness.

Keywords Laser cladding · Ni-based self-fluxing alloy · Powder flow · Coating microstructure · Microhardness

1 Introduction

Laser cladding is one of efficient methods to deposit different coatings on machine parts. In this method, the powder melting and solidification processes lead to the fabrication of single- or multi-layer coatings. Generally, laser cladding can be affected by very large number of factors, and several groups can be identified among them [1–9]. These groups include the following:

- a dependence on laser radiation conditions (laser power, pulse energy, pulse duration, pulse frequency, laser wavelength, laser beam spot diameter, focal distance),

O. Devojno · M. Kardapolava · N. Lutsko
Belarusian National Technical University, Minsk, Belarus

E. Feldshtein (✉)
University of Zielona Góra, Zielona Góra, Poland
e-mail: E.Feldsztein@ibem.uz.zgora.pl

A. Hamrol et al. (eds.), *Advances in Manufacturing*, Lecture Notes in Mechanical Engineering, https://doi.org/10.1007/978-3-319-68619-6_88

- a dependence on conditions of layer forming (laser scan speed, scan strategy rotation, number of spots, scanning space, stripe width, stripe overlap, hatch or track distance, layer thickness, gas content control),
- a dependence on characteristics of powders that was used (size of the powder particles, powder mass flow, temperature of the powder).

A number of studies have been carried out to investigate the properties of single tracks, as well as the coating layer as a whole. In [10], the surface morphology and microstructure of the layer of 316L steel after introduction of a NiB additive were described. The microstructure and nano-mechanical properties of the layer of AlSi10 Mg alloy after selective laser melting were researched in [11], and the density, roughness, and microstructure of AlSi10 Mg layer were described in [12]. The microstructural and mechanical properties and surface quality of CoCrMo alloy and their relationship with some of the selective laser melting parameters were studied in [6, 13] for the surface.

The cladding of self-fluxing alloys on different substrate materials is widely applied. Three groups of these alloys are known now: Fe-based, Ni-based, and Co-based self-fluxing alloys [7, 14–22]. The Ni- and Co-based self-fluxing alloys are characterized by wettability, deoxidization, and by a fluxing effect as well as high physical and mechanical properties, and a good resistance to wear, oxidation, and high-temperature corrosion.

The aim of the present investigation is to study the formation features, microstructure, chemical composition, and microhardness of a NiCrBSi self-fluxing alloy coating formed on AISI 1045 steel's substrate by laser cladding.

2 Experimental Procedure

The research was carried out with Ni-based self-fluxing hard alloy. The chemical composition of the powder and the hardness of the material are shown in Table 1.

The coatings were applied to a substrate of AISI 1045 steel (EN 10277-2-2008 C45 steel). The starting powder was sieved to appropriate granulations using a set of sieves and then was dried in an electric furnace at 200 °C for two hours. Cladding was performed using a continuous-wave CO_2 laser "Comet 2" with the power of 1 kW (Fig. 1). Powder was fed to the work area through a lens with a nozzle for spot coaxial laser cladding which can operate with the CO_2 laser in the range of focal lengths 100–200 mm. The lens can work in conjunction with different gas-powder feeders and provides a simultaneous or programmable flow of up to four different components. The powder components are mixed in a special

Table 1 Powder composition and the material hardness

C (%)	B (%)	Si (%)	Cr (%)	Fe (%)	Ni (%)	Hardness
0.3–0.6	1.7–2.5	1.2–3.2	8–14	1.2–1.3	The rest	HRC 35–40

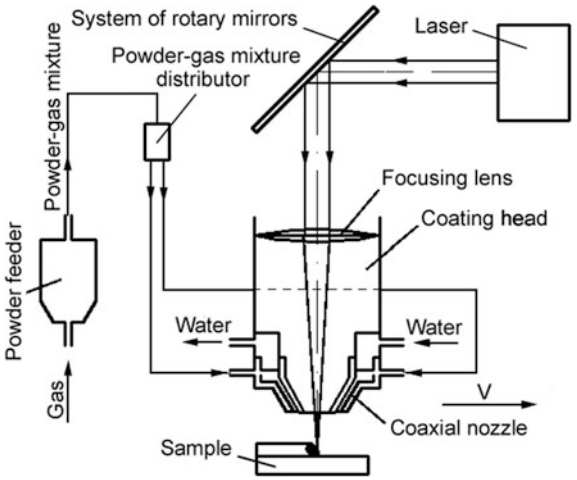

Fig. 1 Scheme of coating deposition

chamber and supplied to the laser target area with the nozzle channels. The lens has an air-cooled lower part of the nozzle and a body that ensures its long service life. The compressed air is used as a transporting gas. The focal length was of 200 mm, and a focused spot was of 1.0 mm.

To determine the optimal particle sizes, the segregation of an in situ powder (Fig. 2) was performed and three fractions were used: less than 20 μ, 20–80 μ and 80–100 μ.

Cladding layers of the Ni-based alloy were tested in the speed range of 40–120 mm/min when the distance between the nozzle and the surface of sample was of 10–14 mm. The diameter of the laser spot was of 1 mm, which corresponds to a power density of 1.27×10^5 W/cm^2.

The powder flow was measured by powder blowing through the feeder nozzle per unit of time when operating the laser, and then samples with deposited powder

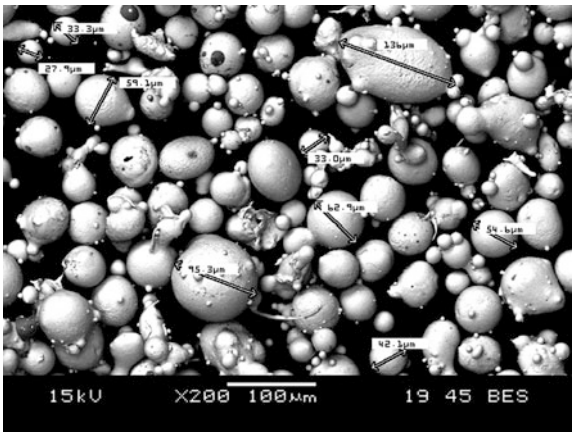

Fig. 2 In situ NiCrBSi powder

were weighed on a CITIZEN CY-124 analytical balance. Compressed air flow was measured with a P5 rotameter with precision ±4%. The air pressure was regulated by a feeder control system. All measurements were repeated three times.

The coating height was measured using an optical microscope with accuracy of 0.001 mm.

The microstructure, morphology, and chemical composition of coatings were analyzed by a scanning electron microscope "Mira." The microhardness was measured using a MICROMET II Hardness Tester. The indenter for Vickers tests with the load of 100 gf was used (further the designation HV 100 was applied).

Statistica 12 software was used for a graphical interpretation of some results.

3 Results and Discussion

3.1 Powder Flow When Passing Through the Nozzle

The research results of the powder passage through the nozzle of the lens are shown in Fig. 3. With increasing gas pressure and gas flow, the flow rate of self-fluxing powder increases, but the behavior of this influence depends on the particle size. In the case of the fraction with particle sizes of 80–100 μm, the effect of the pressure increases, but the intensity of the gas flow effect decreases. For the fraction having particle sizes less than 20 μm, the significant gas flow inhibits the flow rate of particles and the pressure is not affected. This is probably due to packetizing particles in the feeder, which prevents the particles exit from the nozzle. Thus, the powder with the size of 20–80 μm was the best and was accepted for further studies.

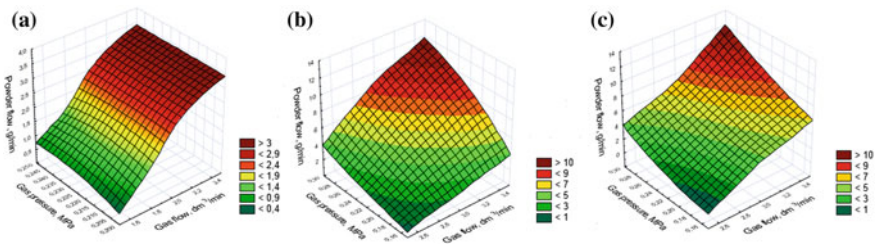

Fig. 3 Efficiency of the powder particles passage with dimensions less than 20 μm (**a**), 20–80 μm (**b**), and 80–100 μm (**c**) through the lens nozzle depending on the pressure and flow of the transporting gas

3.2 *Microstructure and Phase Composition of Single-Layer Coating*

The analysis of the deposited coating layer (Fig. 4) showed that a clear tendency for reducing dimensions of the structural components and the depth of the heat-affected zone is observed with increasing the deposition rate. Favorable conditions for the carbide eutectic γ-Ni–(Cr_3C_2 + Cr_7C_3) formation, as well as the formation of a low-melting eutectic γ-Ni–Ni_3B, whose crystallization occurs in the interdendritic space during cooling, are created in this case.

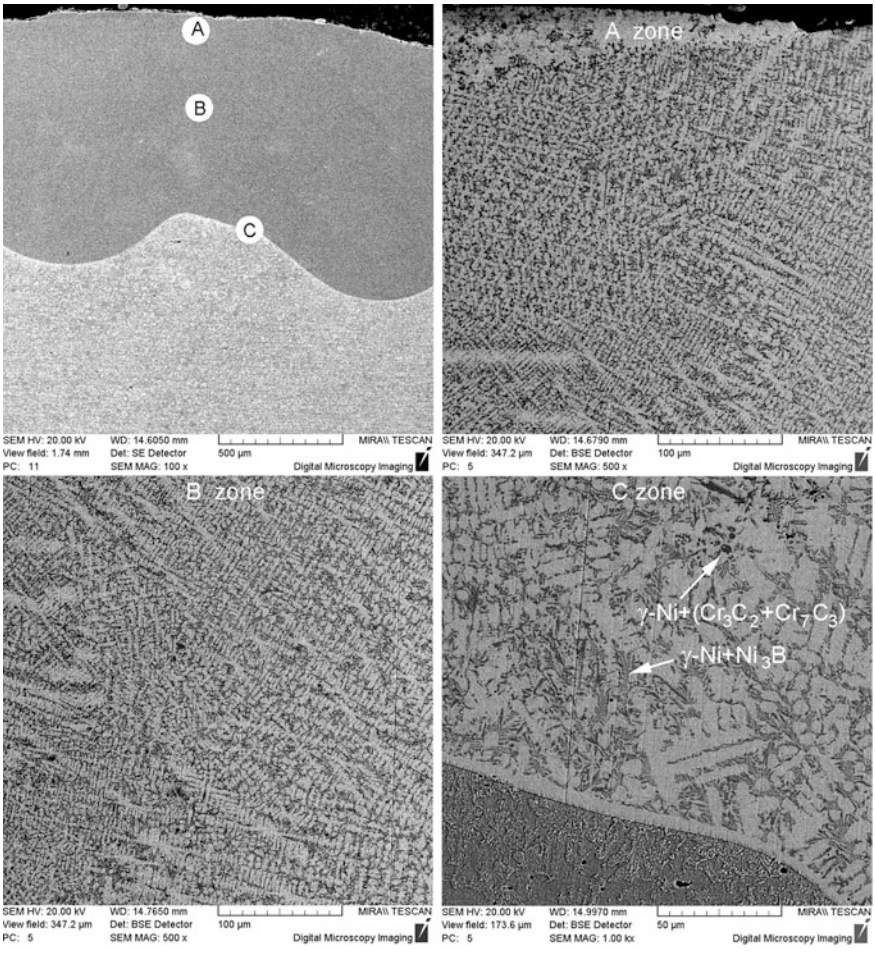

Fig. 4 Microstructure of a coating layer

The cladding distance affects the coating microstructure similarly. Dimensions of the dendrites decrease with its increasing, and their direction is clearly defined only in the upper part of the coating layer.

The differences in the microstructures are caused by the conditions of the heat exchange between the molten coating layer and the substrate. An additional time is required for the reduction of the oxide films when cladding tracks. It includes the recovery time of an oxide film between the substrate and the deposited layer, the recovery time between the powder particles as well as the recovery time of oxides between the tracks. Areas adjacent to a neighboring layer are subjected to the double thermal effect, whereby the sizes of the solid solution dendrites adjacent to the track edge are somewhat increased. The heat-affected zone with the depth of 40–100 μm, depending on deposition conditions, indicates the presence of a chemical bond between the clad layer and the substrate.

With the increase of a laser beam speed and a distance from the nozzle to the coated surface, structural components are crushed, transforming into quasi-eutectic structures. Most of the close-packed planes of a crystal lattice are located on the surface, because dendrites are crystallized at an angle of 45° to it.

As it was noted above, the alloy microstructure consists of two kinds of eutectics: γ-Ni–Ni_3B, whose melting point is 1000 °C, and γ-Ni–(Cr_3C_2 + Cr_7C_3), which crystallizes at higher temperatures and is a strong coating corset. Secondary borides crystallize in the form of small nucleuses and have no time to grow. According to our researches and other investigations [23, 24], the strong coating corset contributes to a high corrosion resistance in alkalis and acids, and low-melting eutectic heals the pores, cracks, and other single defects.

3.3 The Distribution of Elements Over the Depth of a Single-Layer Coating

The results of the study on the elements distribution over the depth of a single-layer coating are shown in Fig. 5. The stable content of the elements was observed practically all over the depth of the coating. The nickel content is about 50% all over the depth of the coating and is much lower than in the in situ powder. At the same time, 40% of the iron is contained in the coating and is also uniformly distributed over the entire depth.

This indicates a significant diffusion of the iron from the substrate since the iron content of the in situ powder does not exceed 1.3% (see Table 1). Chromium and silicon are also uniformly distributed across the depth of the coating and their content corresponds to the in situ powder. The uniform content of elements by coating depth indicates uniform mixing of materials in the melt pond and the same conditions of coating material heating throughout the depth. Nickel, chromium, and silicon do not penetrate from the coating into the substrate.

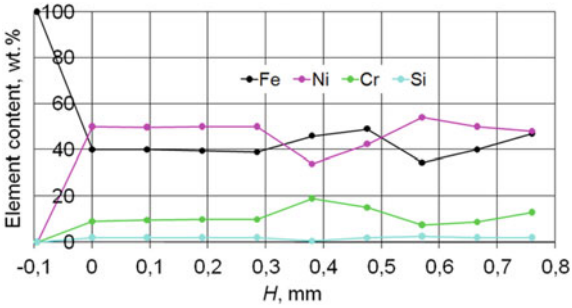

Fig. 5 Distribution of elements at a depth of a coating

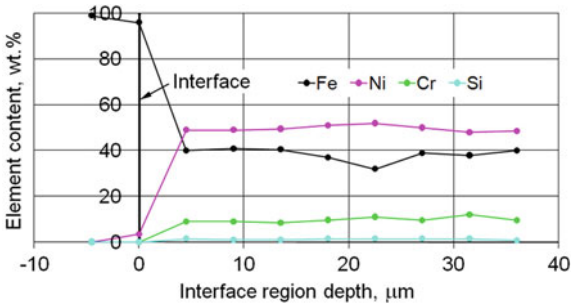

Fig. 6 Distribution of elements in the transient zone of a coating

The finding that the coating elements do not penetrate the substrate is also supported by Fig. 6, which shows the distribution of the elements in the transient zone from the substrate to the coating. Nickel, chromium, and silicon contents are equal to zero already at a depth of 4.5 μm under the interface, and the Ni content was 4% and the Fe content was 95% on the interface. At a height of 4.5 μm above the substrate, the content of elements in the transient zone corresponds to their content all over the depth of the coating.

3.4 Microhardness of the Coating

Microhardness changes by depth and along the coating are shown in Fig. 7. It is easy to notice that the microhardness increases in the "substrate—coating" interface, and then for each cladding condition, it is about at the same level throughout the coating depth (Fig. 8a). Microhardness fluctuations are of HV 100 = 200. Points with an extremely high or extremely low value of microhardness also occur, i.e., HV 100 = 1280 and HV 100 = 200. These changes are caused by the microstructure changes in different areas of the coating.

It is seen from the results of microhardness measurements in the longitudinal direction (Fig. 7b) that for each condition of laser cladding, the microhardness is

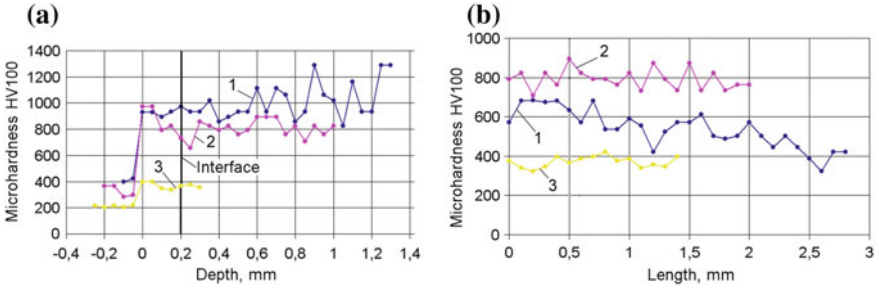

Fig. 7 Changes of microhardness by depth (**a**) and length (**b**) of a coating: 1 – v = 80 mm/min, L = 10 mm, K = 1.0 mm; 2 – v = 120 mm/min, L = 12 mm, K = 1.5 mm; 3 – v = 160 mm/min, L = 12 mm, K = 2.0 mm

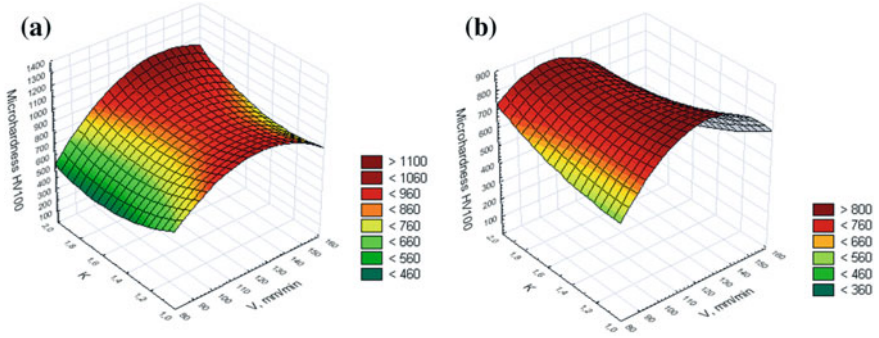

Fig. 8 Effect of laser cladding parameters on the microhardness of coating layer for the distance from the nozzle to the sample surface of L = 10 mm (**a**) and L = 12 mm (**b**)

approximately at the same level all over the length. Fluctuations of microhardness as well as its maximum and minimum values are similar to those in the depth of the single-layer coating.

The effect of laser cladding conditions (speed of the laser beam v, pitch K, and the distance from the nozzle to the sample surface L) on the average microhardness has a complicated character (Fig. 8).

It is known that the crystal growth rate is always less than the nucleation rate and does not depend on the cooling rate and rate of cladding. At the same time, the rate of nucleation of crystals increases with increasing the cooling rate and cladding rate. For this reason, with an increase of the cladding rate from 80 to 120 mm/min, a decrease in the grain sizes and microhardness growth is observed. It is due to the growth of a crystal nucleation rate and to the essentially constant crystal growth rate. With a further increase of the cladding speed to 160 mm/min, despite the continuing reduction in the grains size, the lack of laser power input and a reduction of the fusion strength of grains cause a decrease of the microhardness.

4 Conclusions

Coatings of a Ni-based self-fluxing alloy have been formed by laser cladding using the CW CO_2 laser. The optimal granulation of a self-fluxing alloy powder and the relationship between the flow of powder of various fractions and the flow rate and pressure of the transporting gas have been determined for conditions of coaxial laser cladding. The formation regularities of a single-layer coating microstructure with different cladding conditions as well as patterns of element distribution over the coating depth and in the transient zone are defined. The microhardness distribution patterns by depth and length of the coating for various laser cladding conditions have been studied. It was found that optimal powder grain sizes are of 20–80 μ and reducing dimensions of the structural components and the depth of the heat-affected zone is observed with increasing the speed of the laser beam. The effect of speed of the laser beam, track pitch, and the distance from the nozzle to the coated surface on the average microhardness has a complicated character depended on the cooling conditions.

References

1. Vandenbroucke, B., Kruth, J.-P.: Selective laser melting of biocompatible metals for rapid manufacturing of medical parts. Rapid Prototyping J. **13**, 196–203 (2007)
2. Dimitrov, D., Schreve, K., Beer, N.D.: Advances in three dimensional printing—state of the art and future perspectives. Rapid Prototyping J. **12**, 136–147 (2006)
3. Yadroitsev, I., Bertrand, P., Smurov, I.: Parametric analysis of the selective laser melting process. Appl. Surf. Sci. **253**, 8064–8069 (2007)
4. Ciurana, J., Hernandez, L., Delgado, J.: Energy density analysis on single tracks formed by selective laser melting with CoCrMo powder material. Int. J. Adv. Manuf. Technol. **68**, 1103–1110 (2013)
5. Averyanova, M., Cicala, E., Bertrand, P., Grevey, D.: Experimental design approach to optimize selective laser melting of martensitic 17–4 PH powder: part I—single laser tracks and first layer. Rapid Prototyping J. **18**, 28–37 (2012)
6. Pupo, Y., Monroy, K.P., Ciurana, J.: Influence of process parameters on surface quality of CoCrMo produced by selective laser melting. Int. J. Adv. Manuf. Technol. **80**, 985–995 (2015)
7. Arısoy, Y.M., Criales, L.E., Özel, T., Lane, B., Moylan, S., Donmez, A.: Influence of scan strategy and process parameters on microstructure and its optimization in additively manufactured nickel alloy 625 via laser powder bed fusion. Int. J. Adv. Manuf. Technol. **90**, 1393–1417 (2017)
8. Criales, L.E., Arısoy, Y.M., Lane, B., Moylan, S., Donmez, A., Özel, T.: Predictive modeling and optimization of multi-track processing for laser powder bed fusion of nickel alloy 625. Add. Manuf. **13**, 14–36 (2017)
9. Dunbar, A.J., Denlinger, E.R., Heigel, J., Michaleris, P., Guerrier, P., Martukanitz, R., Simpson, T.W.: Development of experimental method for in situ distortion and temperature measurements during the laser powder bed fusion additive manufacturing process. Add. Manuf. **12**, 25–30 (2016)

10. Stašić, J., Božić, D.: The effect of NiB additive on surface morphology and microstructure of 316L stainless steel single tracks and layers obtained by SLM. Surf. Coat. Technol. **307**, 407–417 (2016)
11. Aboulkhair, N.T., Maskery, I., Tuck, C., Ashcroft, I., Everitt, N.M.: On the formation of AlSi10 Mg single tracks and layers in selective laser melting: Microstructure and nano-mechanical properties. J. Mater. Process. Technol. **230**, 88–98 (2016)
12. Kempen, K., Thijs, L., Van Humbeeck, J., Kruth, J.: Processing AlSi10 Mg by selective laser melting: parameter optimization and material characterization. Mater. Sci. Technol. **31**, 917–923 (2014)
13. Monroy, K.P., Delgado, J., Sereno, L., Ciurana, J., Hendrichs, N.J.: Effects of the selective laser melting manufacturing process on the properties of CoCrMo single tracks. Met. Mater. Int. **20**, 873–884 (2014)
14. Fernández, E., Cadenas, M., González, R., Navas, C., Fernández, R., De Damborenea, J.: Wear behaviour of laser clad NiCrBSi coating. Wear **259**, 870–875 (2005)
15. Chen, H., Xu, C., Qu, J., Hutchings, I.M., Shipway, P.H., Liu, J.: Sliding wear behaviour of laser clad coatings based upon a nickel-based self-fluxing alloy co-deposited with conventional and nanostructured tungsten carbide–cobalt hardmetals. Wear **259**, 801–806 (2005)
16. Wang, X.H., Zhang, M., Liu, X.M., Qu, S.Y., Zou, Z.D.: Microstructure and wear properties of TiC/FeCrBSi surface composite coating prepared by laser cladding. Surf. Coat. Technol. **202**, 3600–3606 (2008)
17. Tong, X., Li, F.-H., Liu, M., Dai, M.-J., Zhou, H.: Thermal fatigue resistance of non-smooth cast iron treated by laser cladding with different self-fluxing alloys. Opt. Laser Technol. **42**, 1154–1161 (2010)
18. Aghasibeig, M., Fredriksson, H.: Laser cladding of a featureless iron-based alloy. Surf. Coat. Technol. **209**, 32–37 (2012)
19. Hemmati, I., Huizenga, R.M., Ocelík, V., De Hosson, J., Th, M.: Microstructural design of hardfacing Ni–Cr–B–Si–C alloys. Acta Mater. **61**, 6061–6070 (2013)
20. Feldshtein, E., Kardapolava, M., Dyachenko, O.: On the effectiveness of multi-component laser modifying of Fe-based self-fluxing coating with hard particulates. Surf. Coat. Technol. **307**, 254–261 (2016)
21. Janka, L., Norpoth, J., Eicher, S., Ripoll, M.R., Vuoristo, P.: Improving the toughness of thermally sprayed Cr 3C 2-NiCr hardmetal coatings by laser post-treatment. Mater. Des. **98**, 135–142 (2016)
22. Krolczyk, G.M., Nieslony, P., Krolczyk, J.B., Samardzic, I., Legutko, S., Hloch, S., Barrans, S., Maruda, R.W.: Influence of argon pollution on the weld surface morphology. Measurement **70**, 203–213 (2015)
23. Paulin, C., Chicet, D.L., Istrate, B., Panțuru, M., Munteanu, C.: Corrosion behavior aspects of Ni-base self-fluxing coatings. IOP Conf. Ser. Mater. Sci. Eng. **147**, 012034 (2016)
24. Sadeghimeresht, E., Markocsan, N., Nylén, P.: Microstructural characteristics and corrosion behavior of HVAF- and HVOF-sprayed Fe-based coatings. Surf. Coat. Technol. **318**, 365–373 (2017)